J Electroceram (2010) 24:300–307
DOI 10.1007/s10832-009-9572-0

Study of bulk and grain-boundary conductivity of $Ln_{2+x}Hf_{2-x}O_{7-\delta}$ (Ln = Sm-Gd; x = 0, 0.096) pyrochlores

A. V. Shlyakhtina · S. N. Savvin · A. V. Levchenko · A. V. Knotko · Petra Fedtke · Andreas Busch · Torsten Barfels · Marion Wienecke · L. G. Shcherbakova

Received: 15 January 2008 / Accepted: 1 April 2009 / Published online: 9 May 2009

Abstract The electrical conductivity of new solid electrolytes $Eu_{2.096}Hf_{1.904}O_{6.952}$ and $Gd_2Hf_2O_7$ have been compared with those for different pyrochlores including titanates and zirconates $Ln_{2+x}M_{2-x}O_{7-\delta}$ (Ln = Sm-Lu; M = Ti, Zr; x= 0−0.81). Impedance spectroscopy data demonstrate that $Eu_{2.096}Hf_{1.904}O_{6.952}$ and $Gd_2Hf_2O_7$ synthesized from mechanically activated oxides have high ionic conductivity, comparable to that of their zirconate analogues. The bulk and grain-boundary components of conductivity in $Sm_{2.096}Hf_{1.904}O_{6.952}$ (T_{synth}=1600ºC), $Eu_{2.096}Hf_{1.904}O_{6.952}$ and $Gd_2Hf_2O_7$ (T_{synth}=1670ºC) have been determined. The highest bulk conductivity is offered by the disordered pyrochlores prepared at 1600ºC and 1670ºC: ~1.5×10^{-4} S/cm for $Sm_{2.096}Hf_{1.904}O_{6.952}$, 5×10^{-3} S/cm for $Eu_{2.096}Hf_{1.904}O_{6.952}$ and 3×10^{-3} S/cm for $Gd_2Hf_2O_7$ at 780ºC, respectively. The conductivity of the fluorite-like phases at the phase boundaries of the $Ln_{2+x}M_{2-x}O_{7-\delta}$ (Ln = Eu, Gd; M = Zr, Hf; x~0.286) solid solutions, as well as that of the high-temperature fluorite-like phases $Ln_{2+x}M_{2-x}O_{7-\delta}$ (Ln = Eu, Gd; M = Zr, Hf; x = 0−0.286), is lower than the conductivity of the disordered pyrochlores $Ln_{2+x}M_{2-x}O_{7-\delta}$ (Ln = Eu, Gd; M = Zr, Hf; x=0−0.096).

Keywords Pyrochlore · Fluorite · Total conductivity · Ionic conductivity · Mixed conductivity

A. V. Shlyakhtina (✉) · L. G. Shcherbakova
Semenov Institute of Chemical Physics,
Russian Academy of Sciences,
ul. Kosygina 4,
Moscow 119991, Russia
e-mail: annashl@inbox.ru
e-mail: annash@chph.ras.ru

S. N. Savvin · A. V. Knotko
Faculty of Chemistry, Moscow State University,
Leninskie gory 1,
Moscow 119991, Russia

A. V. Levchenko
Institute of Problems of Chemical Physics,
Russian Academy of Sciences,
Akad. N.N. Semenov avenue,
Moscow, Russia

P. Fedtke · A. Busch · T. Barfels · M. Wienecke
Hochschule Wismar Institute of Surface and Thin Film Technology, Philipp-Muller-Strasse,
23952 Wismar, Germany

1 Introduction

Mixed oxides possessing high oxygen ion conductivity typically undergo order-disorder (OD) phase transitions involving an increase in oxygen vacancy concentration. Studies of OD transitions on a microscopic scale from lattice defects to superstructure microdomains nucleating in the bulk of the parent phase are an effective approach to gaining insight into the mechanisms of ionic conduction in various oxides. Ln_2O_3-MO_2 (Ln = Sm−Gd; M = Zr, Hf) oxides are known to undergo a pyrochlore-fluorite OD phase transition [1, 2].

Oxygen ion conduction in the Ln_2O_3-HfO_2 (Ln = Nd, Sm-Gd) systems has been studied in less detail compared to the Ln_2O_3-ZrO_2 (Ln = Nd, Sm-Gd) systems. The reason for this is that $Ln_{2\pm x}Zr_{2\pm x}O_{7\pm\delta}$ solid solutions are high-temperature oxygen ion conductors with significant compositional disorder and contain considerable concentrations of oxygen vacancies and/or interstitials [1–4]. Even though zirconium and hafnium differ very little in ionic radius ($R_{Zr\ c.n.\ 6}^{4+}$ = 0.72 Å; $R_{Hf\ c.n.\ 6}^{4+}$ = 0.71 Å), Hf-O bonds are more covalent than Zr-O because Hf has a filled $4f^{14}$ shell, which ensures a more significant overlap of electron

orbitals by virtue of its structure. As a result, the hafnates are less prone to defect formation and have significantly lower oxygen ion conductivity than do the zirconates [5]. The same is true for rare-earth stannates. Attempts to raise the ionic conductivity of $Y_2Ti_2O_7$ via replacement of Ti^{4+} with the larger cation Sn^{4+}, intermediate in radius between Ti^{4+} and Zr^{4+}, for $Y_2(Sn_yTi_{1-y})_2O_7$ series were unsuccessful in [6]. $Y_2Sn_2O_7$ remained fully ordered in the temperature range 25–1450ºC. Clearly, in addition to the relationship between the radii of the A and B cations, the B^{4+}–O bond covalence is of importance. In particular, the Sn^{4+}–O bond in $Y_2Sn_2O_7$ is far stronger than the B^{4+}–O bond in$Y_2(Zr_{0.6}Ti_{0.4})_2O_7$ [6]. The ionic conductivity in the $Gd_2(Sn_yTi_{1-y})_2O_7$ system was also reported to drop for $y>0.4$, like that in the $Y_2(Sn_yTi_{1-y})_2O_7$ system.

Interesting results were obtained by Moreno et al. [7], who used mechanically activated oxides in $Gd_2(Sn_yZr_{1-y})_2O_7$ preparations. Moreno et al. [7, 8] obtained $Gd_2(Sn_yZr_{1-y})_2O_7$ and $Dy_2(Ti_{1-y}Zr_y)_2O_7$ by firing mechanically activated oxides at 1500ºC for 36 h. Ionic conductivity measurements showed a jump in conductivity for $y>0.4$, similar to what was reported for $Y_2(Zr_yTi_{1-y})_2O_7$ [6]. The Zr^{4+}–O bond in $Gd_2(Sn_yZr_{1-y})_2O_7$ is far weaker than the Ti^{4+}–O bond in $Gd_2(Sn_yTi_{1-y})_2O_7$. Thus, those results provide further evidence that the reducing of the B^{4+}–O bond covalence is of importance for defect formation.

The first syntheses of $Ln_{2+x}Hf_{2-x}O_{7-\delta}$ (x=0.096; Ln = Sm, Eu) and $Gd_2Hf_2O_7$ with the use of mechanical activation, which seems to favour the formation of anti-site defects in cubic oxides, were reported in [9]. The materials were found to have high conductivity, approaching that of their zirconate analogues. The cation disorder in the hafnates, quantified by the density of $Ln_{Hf}^{'} + Hf_{Ln}^{\bullet}$ defects, was close to that in the zirconates [9]. The $Sm_{2.096}Hf_{1.904}O_{6.952}$ solid solution has a pyrochlore-like structure over the entire temperature range studied, from 1000ºC to 1670ºC, whereas $Eu_{2.096}Hf_{1.904}O_{6.952}$ and $Gd_2Hf_2O_7$ undergo a transformation from a low-temperature fluorite-like phase to a pyrochlore-like phase at 1200ºC, accompanied by a rise in conductivity. Measurements in that study were performed only at a limited number of frequencies [9], so that the bulk and grain-boundary components of conductivity could not be assessed separately. In this paper, we present a more detailed study of $Sm_{2.096}Hf_{1.904}O_{6.952}$, $Eu_{2.096}Hf_{1.904}O_{6.952}$ and $Gd_2Hf_2O_7$. Samples synthesized at 1600ºC or 1670ºC were characterized by impedance spectroscopy with the aim of determining the bulk (intragranular) and grain-boundary components of conductivity.

The conductivity of new solid electrolytes $Eu_{2.096}Hf_{1.904}O_{6.952}$ and $Gd_2Hf_2O_7$ has been compared with conductivity of titanates and zirconates pyrochlores $Ln_{2+x}M_{2-x}O_{7-\delta}$ (Ln = Sm−Lu; M = Ti, Zr; x=0−0.096).

2 Experimental

$Ln_{2.096}Hf_{1.904}O_{6.952}$ (Ln = Sm, Eu) and $Gd_2Hf_2O_7$ were synthesized from Ln_2O_3 and HfO_2 powders mechanically activated in an eccentric vibratory mill with a 120 cm^3 vial volume [10]. The sample weight was 21 g, the ball-to-powder weight ratio was ~15, and the vibration amplitude and frequency were 0.5 cm and 50 Hz.

In conductivity measurements, we used disc-shaped samples 10 mm in diameter and 2.5–3 mm in thickness, prepared by pressing the milled powders at 20–22 MPa, followed by heat treatment at 1200ºC for 24 h, at 1600ºC for 4 h or at 1670ºC for 2 h.

Conductivity was determined by impedance spectroscopy (Zahner IM6E bridge) at frequencies from 0.01 Hz to 1 MHz. The measurements were made in the temperature range 300–1000ºC at an oxygen pressure of 10^5 Pa. The same bridge was used to assess the electronic conductivity of the $Sm_{2.096}Hf_{1.904}O_{6.952}$ sample synthesized at 1600ºC. The resistance of the sample was measured at dc by the Hebb-Wagner method.

For some of the samples, we performed two-probe measurements in a NorECs ProboStat cell. The signal was monitored with a Beta-N impedance analyser at frequencies from 10 mHz to 3 MHz and temperatures from 400ºC to 900ºC. The applied voltage was 0.5 V, and the conductivity was determined to within 5% accuracy. Electrical contacts were made by applying ChemPure C3605 Pt paste followed by firing at 1000ºC for 30 min.

The ceramics were characterized by x-ray diffraction (XRD) on a DRON-3M automatic diffractometer (Cu K $_\alpha$; 2Θ=15–65°).

$Sm_{2.096}Hf_{1.904}O_{6.952}$ was examined by electron diffraction on a JEOL JEM-2000FXII.

3 Results and discussion

The XRD patterns of the $Sm_{2.096}Hf_{1.904}O_{6.952}$ samples prepared at 1200ºC, 1600ºC and 1670ºC are shown in Fig. 1. Note, first of all, the presence of very weak pyrochlore superstructure peaks ((111), (311), (331) (almost indiscernible), (511)) and strong fluorite substructure peaks. Similar diffraction patterns were obtained earlier for $Eu_{2.096}Hf_{1.904}O_{6.952}$ and $Gd_2Hf_2O_7$ [9]. This type of XRD pattern, with weak superstructure peaks, was also reported for pyrochlore-like $Ln_{2+x}Zr_{2-x}O_{7-\delta}$ in Ln_2O_3-ZrO_2 systems [11, 12]. The materials were assumed to have an anti-phase microdomain structure in a certain range of Ln_2O_3 contents, resulting in a sharp drop in the intensity of the pyrochlore superstructure peaks. Deviations from stoichiometry in $Gd_{2+x}Zr_{2-x}O_{7-\delta}$ were hypothesized to be compensated through the formation of anti-phase microdomain bound-

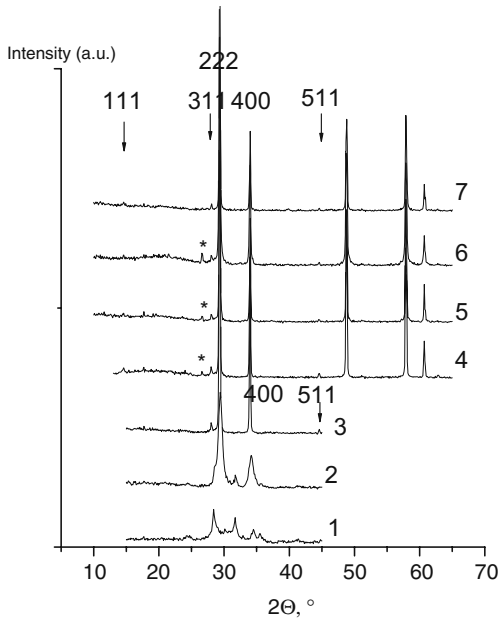

Fig. 1 XRD patterns of an Sm_2O_3 +2 HfO_2 mixture mechanically activated at 25ºC (1) and $Sm_{2.096}Hf_{1.904}O_{6.952}$ samples heat-treated at 1000ºC (2), 1200ºC (3), 1300ºC (4), 1450ºC (5), 1600ºC (6) and 1670ºC (7)

aries [13]. The coordination number of the Gd cations near the anti-phase boundaries was assumed to be below 8, in contrast to the octahedral coordination of lanthanides in the pyrochlore structure [13]. Last investigations of titanates Ln_2TiO_5 (pyrochlore structure) show that the low intensity of the pyrochlore superstructure reflections is due to the small size of pyrochlore microdomains embedded in fluorite matrix [14]. The possibility of the observation of that microdomain stucture by electron microscopy often has limited by technical level of the electron microscope type.

Figure 2(a) shows the 300ºC and 400ºC impedance spectra of the $Sm_{2.096}Hf_{1.904}O_{6.952}$ sample synthesized at 1600ºC. In the inset of Fig. 2(a), one can clearly see two semicircles, corresponding to the bulk (high frequencies) and grain-boundary (medium frequencies) components of conductivity, and the portion representing conduction across the sample-electrode interface. Clearly, at these low temperatures, the conductivity is determined by the grain-boundary component. With increasing temperature, however, the grain-boundary component of resistance decreases considerably more rapidly than the bulk component. Figure 2(b) shows the 600ºC impedance spectra of the $Sm_{2.096}Hf_{1.904}O_{6.952}$ samples synthesized at 1200ºC, 1600ºC and 1670ºC. In the three spectra, the high- to medium-frequency arc is a combination of the semicircles due to the bulk (intragranular) and grain-boundary components of conductivity. The low-frequency arc represents charge transport across the electrode-sample interface. In contrast to the low-temperature spectra, the 600ºC grain-boundary and bulk charge transport processes are very close in parameters, as evidenced by the significant overlap of the semicircles representing these processes. In the three spectra, the significant overlap of the bulk and grain-boundary components of conductivity makes it difficult to separately evaluate them. At higher temperatures, this is impossible. Electronic conductivity of the $Sm_{2.096}Hf_{1.904}O_{6.952}$ assessed by Hebb-Wagner technique was at least three orders of magnitude lower then the ionic component.

Figure 3(a) presents the Arrhenius plots of the bulk and grain-boundary components of conductivity for the $Sm_{2.096}Hf_{1.904}O_{6.952}$ prepared at 1600ºC. Note that the activation energy for bulk conduction is as low as 0.55 eV, whereas that for grain-boundary conduction is 0.97 eV. This low activation energy for bulk conduction is atypical of oxygen ion conductors. However, for pyrochlores, this is not so special. Further lower activation energy of 0.51 eV was reported in [15]. Figure 3(b, c) shows the Arrhenius plots of bulk and grain-boundary conductivities for the $Eu_{2.096}Hf_{1.904}O_{6.952}$ and $Gd_2Hf_2O_7$ samples synthesized at 1670ºC. The impedance spectroscopy data demonstrate that these samples have high conductivities: 5×10^{-3} и 3×10^{-3} S/cm, respectively, at 780ºC. The bulk conductivity of $Eu_{2.096}Hf_{1.904}O_{6.952}$ is notably higher than its grain-boundary conductivity over the entire temperature range studied, up to 1000ºC. So the bulk conductivity of $Sm_{2.096}Hf_{1.904}O_{6.952}$ is lower the conductivity of $Eu_{2.096}Hf_{1.904}O_{6.952}$ and $Gd_2Hf_2O_7$ samples. The data [9], obtained only at a limited number of frequencies, were confirmed by impedance spectroscopy data in this investigation.

Grain size and density data for the materials studied are presented at Fig. 4. The average grain size of the $Ln_{2.096}Hf_{1.904}O_{6.952}$ (Ln = Sm, Eu) samples is 1–2 μm as determined by SEM. $Gd_2Hf_2O_7$ consists of both coarse (3–4 μm) and fine (≈200 nm) grains. The relative densities of $Sm_{2.096}Hf_{1.904}O_{6.952}$ and $Eu_{2.096}Hf_{1.904}O_{6.952}$ reach 95.5% and 97.8%, respectively; that of $Gd_2Hf_2O_7$ is slightly lower, 92.3%. SEM data correlate with the above relationship between the bulk and grain boundary conductivities of our samples. The large grain size of $Gd_2Hf_2O_7$ leads to a higher grain boundary conductivity, whereas in $Ln_{2.096}Hf_{1.904}O_{6.952}$ (Ln = Sm, Eu) the bulk conductivity exceeds the grain boundary conductivity.

Figure 5(a) shows the total conductivity for $Gd_2Hf_2O_7$, $Eu_{2.096}Hf_{1.904}O_{6.952}$ and $Sm_{2.096}Hf_{1.904}O_{6.952}$ samples obtained at 1200ºC, 1600ºC and 1670ºC according [9]. Figure 5(b) shows the anti-structure pairs $Ln_{Hf}^{'} + Hf_{Ln}^{\bullet}$ and $Ln_{Hf}^{'}$ defects number for samples synthesized at 1600ºC. Best ion-conducting samples $Gd_2Hf_2O_7$, $Eu_{2.096}Hf_{1.904}O_{6.952}$ have 8–16% anti-structure pairs $Ln_{Hf}^{'} + Hf_{Ln}^{\bullet}$ at the room temperature. $Sm_{2.096}Hf_{1.904}O_{6.952}$ obtained at 1600ºC and 1670ºC didn't show anti-structure pairs $Sm_{Hf}^{'} + Hf_{Sm}^{\bullet}$ and its

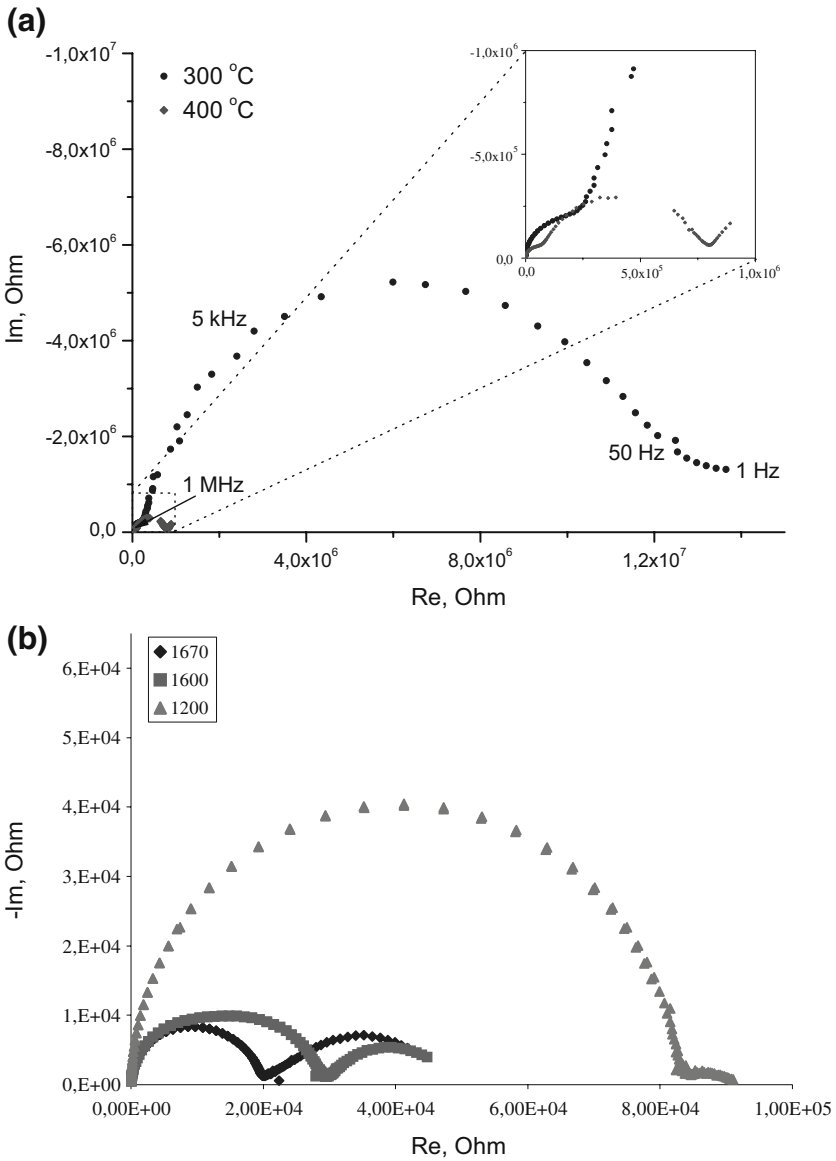

Fig. 2 (**a**) 300ºC and 400ºC impedance spectra of the $Sm_{2.096}Hf_{1.904}O_{6.952}$ sample synthesized at 1600ºC and (**b**) 600ºC impedance spectra of the $Sm_{2.096}Hf_{1.904}O_{6.952}$ samples synthesized at 1200ºC, 1600ºC and 1670ºC

total conductivity is one order magnitude lower then that of $Gd_2Hf_2O_7$. The results [16] showed that Ln'_{Ti} and $Ti_{Ln}^{\bullet}$ defects form easily in rare-earth titanates in the heating process and often disappear in the cooling process. We have another situation for $Gd_2Hf_2O_7$, $Eu_{2.096}Hf_{1.904}O_{6.952}$ in this work. Ln_{Hf}' and $Hf_{Ln}^{\bullet}$ defects induced by mechanical activation with subsequent sintering at high temperature 1600–1670ºC in hafnates were preserved during the cooling down to the room temperature.

In this context, it should be discussed the mechanical activation and its role in the generation of anti-site defects in the pyrochlore structure. The high-conductivity DP phase of the $Ln_2Ti_2O_{7-\delta}$ titanates contains $Ln'_{Ti} + Ti^{\bullet}_{Ln}$ anti-structure pairs and oxygen vacancies in the temperature range of our conductivity measurements (450–950ºC). These defects may relax during cooling or storage if the samples were synthesized using co-precipitation [17]. Similar results were reported by Eberman et al. [16] for $(Sc_zYb_{1-z})_2Ti_2O_7$. However, in the synthesis of titanates with the use of mechanical activation followed by firing, $Ln'_{Ti} + Ti^{\bullet}_{Ln}$ cation defects may be stabilized, as was found for $Yb_2Ti_2O_7$, which was shown to contain about 4.5% $Yb'_{Ti} + Ti^{\bullet}_{Yb}$ anti-structure pairs at room temperature [17]. In the $Ln_{2+x}M_{2-x}O_{7-\delta}$ (Ln = Sm–Gd; M = Zr, Hf; x=0–0.286) systems, anti-structure pairs (5–22%) were found at room temperature in $Ln_2M_2O_7$ (M = Zr, Hf) samples synthesized using mechanical activation [9]. The relaxation of anti-site defects in the $Ln_2Ti_2O_7$ titanates during cooling or room-temperature storage and their stability in the $Ln_2M_2O_7$ (M = Zr, Hf) materials suggest that anti-structure pairs are more stable at a smaller difference in ionic radius between Ln^{3+} and M^{4+}. In

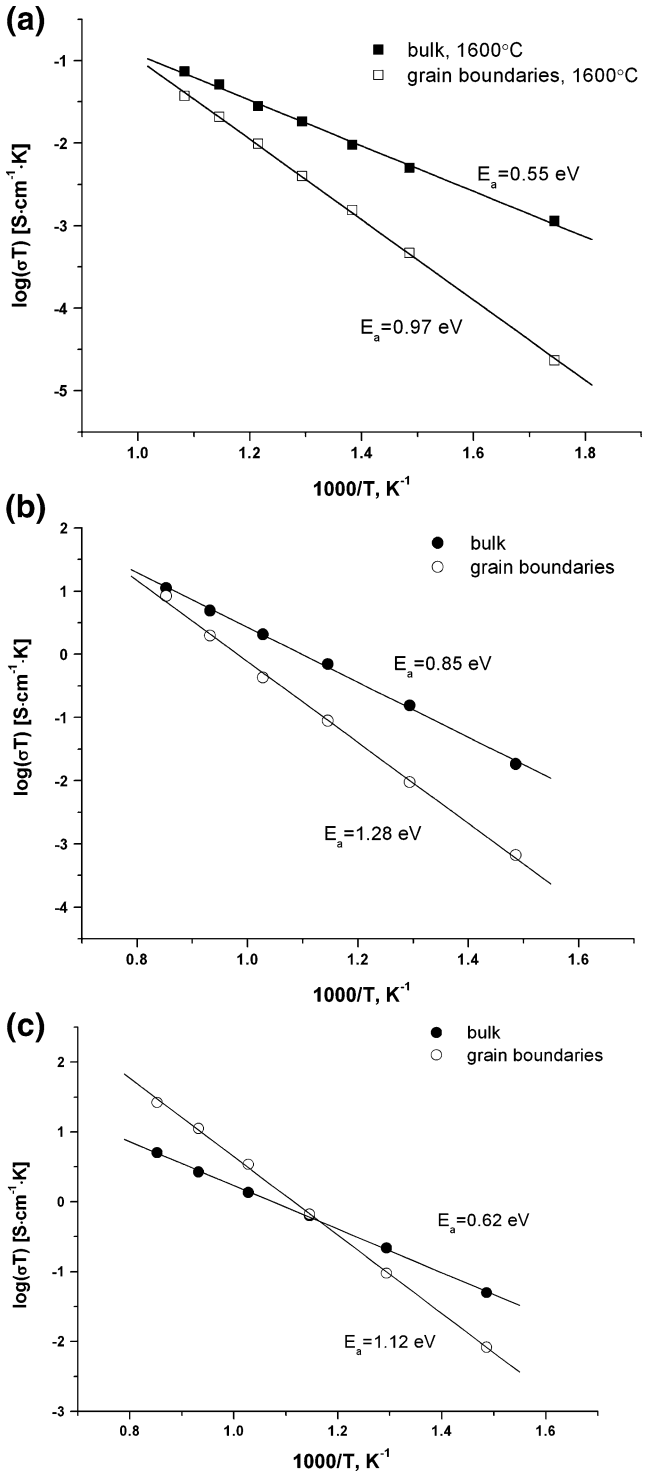

Fig. 3 (**a**) Arrhenius plots of the bulk and grain-boundary components of conductivity for the $Sm_{2.096}Hf_{1.904}O_{6.952}$ sample synthesized at 1600ºC, (**b**) Arrhenius plots of bulk and grain-boundary conductivities for the $Eu_{2.096}Hf_{1.904}O_{6.952}$ and (**c**) $Gd_2Hf_2O_7$ samples synthesized at 1670ºC

particular, the difference is 0.38 Å (the largest) in the titanates, 0.346 Å in the zirconates and 0.343 Å in the hafnates. In a recent paper, Fuentes et al. [18] have described the synthesis of lanthanide titanate pyrochlores through mechanical processing in a planetary mill, which demonstrates that mechanochemical synthesis of pyrochlores does occur at room temperature. Thus, both anti-site defects and oxygen vacancies can be produced by mechanical processing. Clearly, subse-

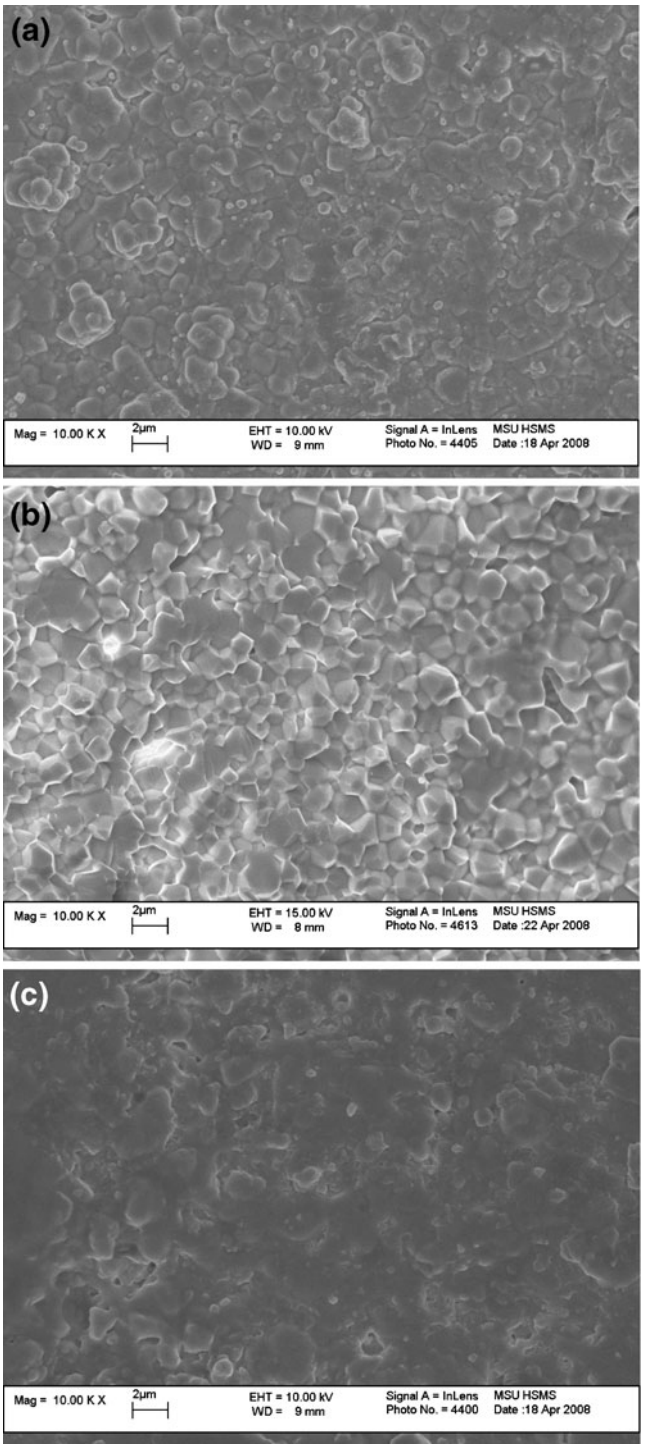

Fig. 4 SEM pictures for $Sm_{2.096}Hf_{1.904}O_{6.952}$ 1600ºC (**a**), $Eu_{2.096}Hf_{1.904}O_{6.952}$ 1670ºC (**b**), $Gd_2Hf_2O_7$ 1670ºC (**c**)

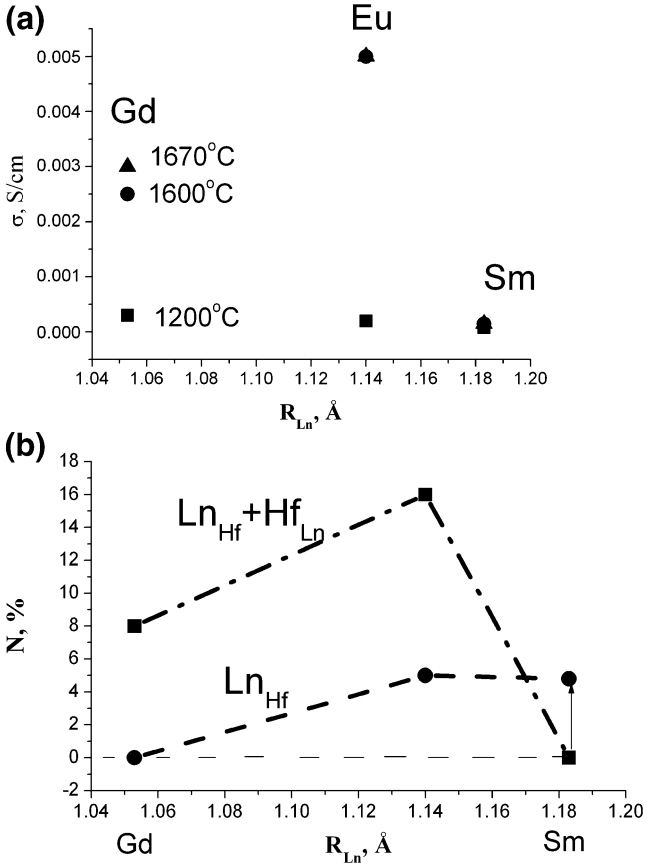

Fig. 5 Total conductivity (**a**) and $Ln_{Hf}^{'} + Hf_{Ln}^{\bullet}$ anti-structure pairs and Ln_{Hf} defects (**b**) for $Sm_{2.096}Hf_{1.904}O_{6.952}$, $Eu_{2.096}Hf_{1.904}O_{6.952}$ and $Gd_2Hf_2O_7$ samples synthesized at 1600ºC

quent high-temperature heat treatment influences the defect structure of the titanates. At the same time, the fact that defects (4.5%) were found in $Yb_2Ti_2O_7$ at room temperature after high-temperature synthesis from a mechanically activated mixture [17] suggests that mechanical activation may produce defects in appropriate symmetrical structures and that some of the defects may persist after high-temperature annealing. Since the M^{4+}–O bonds in the hafnates and zirconates are less covalent than those in the titanates [19], mechanical activation of $Ln_2M_2O_7$ (Ln = Sm − Gd; M = Zr, Hf) is also quite likely to produce anti-site defects.

As it was stated before, among the $Ln_{2+x}M_{2-x}O_{7-\delta}$ (Ln = Sm–Gd; M = Zr, Hf) solid solutions lying in the homogeneity range of the pyrochlore phases $Ln_2M_2O_7$ (M = Zr, Hf), the highest conductivity is offered by nominally stoichiometric compounds with a distorted pyrochlore structure (this phase has $Ln_{Hf}^{'}$ and $Hf_{Ln}^{\bullet}$ defects) and by pyrochlore-like solid solutions with small deviations from stoichiometry [2, 9].

Clearly, the high-temperature phases of $Ln_2M_2O_7$ (Ln = Sm–Gd; M = Zr, Hf) have the optimal concentration and mobility of oxygen vacancies, which are generated according to the schemes:

$$Ln_{Ln}^{x} + M_M^{x} \rightarrow Ln_M^{'} + M_{Ln}^{\bullet} \quad (1)$$

$$O_o^{x} \rightarrow V_{O(48f)}^{\bullet\bullet} + O_{i(8b)}^{''} \quad (2)$$

The excess Ln^{3+} ions in $Ln_{2+x}M_{2-x}O_{7-\delta}$ (Ln = Sm–Gd; M = Zr, Hf) are presumably accommodated in the M^{4+} site; i.e., the general formula can be written in the form $Ln_2(M_{2-x}Ln_x)O_{7-\delta}$. Residing in the B site of the pyrochlore ($A_2B_2O_7$) structure, Ln^{3+} favors the formation of oxygen vacancies according to the scheme:

$$Ln_2O_{3\rightarrow MO2} \rightarrow 2(Ln_M)^{'} + V_{O(48f)}^{\bullet\bullet} + 3O_O^{x} \quad (3)$$

The oxygen vacancy concentration must, therefore, increase with *x*.

However, like in the $Ln_{2+x}Ti_{2-x}O_{7-x/2}$ (Ln = Er–Lu) solid solutions, the conductivity was found to decrease with increasing Ln content. This is, most likely, due to Ln − vacancy association according to the scheme:

$$Ln_M^{'} + V_O^{\bullet\bullet} \leftrightarrow (Ln_M V_O)^{\bullet} \quad (4)$$

High Ln contents lead to the formation of defect clusters, which contain both cation anti-structure pairs and anion pairs (Frenkel defects):

$$Ln_{Ln}^{x} + M_M^{x} + O_o^{x} \rightarrow \left\{ Ln_M^{'} + M_{Ln}^{\bullet} + V_{O(48f)}^{\bullet\bullet} + O_{i(8b)}^{''} \right\}^{x} \quad (5)$$

It seems likely that the reduction in ionic conductivity with increasing Ln content is due to a decrease in carrier mobility rather than to a decrease in carrier concentration. The conductivity of heavily doped fluorite-like phases at the pyrochlore-fluorite phase boundary, as well as that of the high-temperature fluorite-like phases $Ln_2M_2O_7$ (M = Zr, Hf), is always lower than the conductivity of the distorted pyrochlores and pyrochlore-like solid solutions.

The same results follow from the data reported by van Dijk et al. [2]. In that work, a single crystal of composition $Gd_{0.52}Zr_{0.48}O_{1.74}$, lying in the pyrochlore-like solid-solution region, with an excess of Gd_2O_3, was quenched from the synthesis temperature (~2500ºC) and then annealed for 20 h at 1250ºC, i.e., well below 1530ºC, the temperature of the pyrochlore-fluorite OD phase transition (sample A). Sample A and a sample of the same composition (B) quenched from the synthesis temperature (2500ºC) were characterized by XRD. Pyrochlore superstructure peaks were only detected in the XRD pattern of sample A, while that of sample B showed only fluorite substructure peaks. Conductivity measurements showed

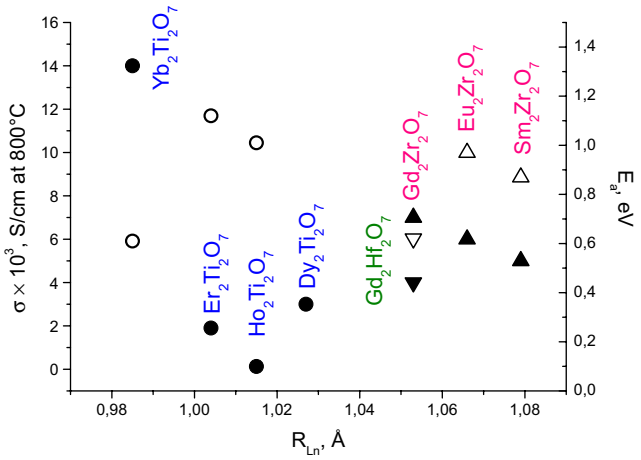

Fig. 6 Ionic conductivity (*filled data points*) and activation energy (*open data points*) as functions of the radius of the lanthanide for $Ln_2M_2O_7$ (Ln = Sm–Lu; M = Ti, Zr, Hf)

that the pyrochlore-structured crystal (sample A) had a higher bulk conductivity and lower activation energy in comparison with sample B. In later studies of the high-temperature OD transition in polycrystalline $Gd_2Zr_2O_7$ (T_{OD}=1530°C) [12], the fluorite-like phase quenched from 1700ºC, i.e., from above the transition temperature, contained pyrochlore microdomains and was, in fact, a heavily disordered pyrochlore rather than a pure fluorite. That material had a lower bulk conductivity in comparison with the material synthesized at 1550ºC, which had a slightly distorted pyrochlore structure.

Present investigation shows that the new solid electrolytes $Gd_2Hf_2O_7$ and $Eu_{2.096}Hf_{1.904}O_{6.952}$ can be included in the high temperature conducting pyrochlores $Ln_{2+x}M_{2-x}O_{7-x/2}$ (Ln = Sm–Lu; M = Ti, Zr, Hf) family.

At least we would like to discusse the temperature effect on conductivity of the pyrochlore-like $Ln_{2+x}M_{2-x}O_{7-x/2}$ (Ln = Sm–Lu; M = Ti, Zr, Hf).

Raising the temperature influences:

(1) the generation of anti-site defects and oxygen vacancies,
(2) oxide ion mobility,
(3) metal–oxygen (M^{4+}–O) bond covalency.

The cation radius difference, ΔR, influences the generation of anti-site defects and oxygen vacancies: the smaller the difference, the higher the probability of the formation of anti-structure pairs and oxygen vacancies. With increasing temperature, the concentration of anti-structure pairs increases.

The M^{4+}–O bond covalency decreases in the order Sn^{4+}–O > Ti^{4+} –O > Hf^{4+} –O > Zr^{4+} –O [19]. This implies that the Zr^{4+}–O bond has the greatest tendency to break, leading to defect formation in the pyrochlore structure. With increasing temperature, the tendency for M^{4+}–O bonds to break becomes more pronounced in the same order.

Our results (Figs. 6, 7) demonstrate that, among the $Ln_{2+x}M_{2-x}O_{7-\delta}$ (Ln = Sm – Lu; M = Ti, Zr, Hf; x=0–0.81) materials studied, the highest conductivity is offered by $Yb_2Ti_2O_7$ and $Yb_{2+x}Ti_{2-x}O_{7-\delta}$ (x=0.096) solid solution as well as $Eu_{2.096}Hf_{1.904}O_{6.952}$ and $Gd_{2.096}Zr_{1.904}O_{6.952}$. At the same time, the cation radius difference in $Yb_2Ti_2O_7$ (0.38 Å) is greater than that in the high-conductivity $Eu_2M_2O_7$ with M = Zr and Hf (0.346 Å in the zirconates and 0.356 Å in the hafnates), and the Ti^{4+}–O bond covalency is the highest among the M^{4+}–O bonds in $Ln_{2+x}M_{2-x}O_{7-\delta}$ (M = Ti, Zr, Hf). Our measurements were performed in the range 300–1000ºC. Thus, with increasing temperature the highest conductivity is offered by compounds in which ΔR and bond covalency are far from being the lowest. The relationship seems to be more complex. We believe that the small cation size is also essential.

4 Conclusions

The electrical conductivity of pyrochlore-like $Ln_{2.096}Hf_{1.904}O_{6.952}$ (Ln = Sm, Eu) solid solutions and $Gd_2Hf_2O_7$ synthesized in the range 1600–1670ºC using mechanical activation was determined for the first time by impedance spectroscopy. $Eu_{2.096}Hf_{1.904}O_{6.952}$ and $Gd_2Hf_2O_7$ pyrochlores are shown to have high ionic conductivity according to its energy activation (0.85 eV and 0.62 eV, respectively), comparable to that of their zirconate analogues. The highest conductivity is offered by pyrochlores slightly disordered in both the anion and cation sublattices. The conductivity of the high-temperature fluorite-like

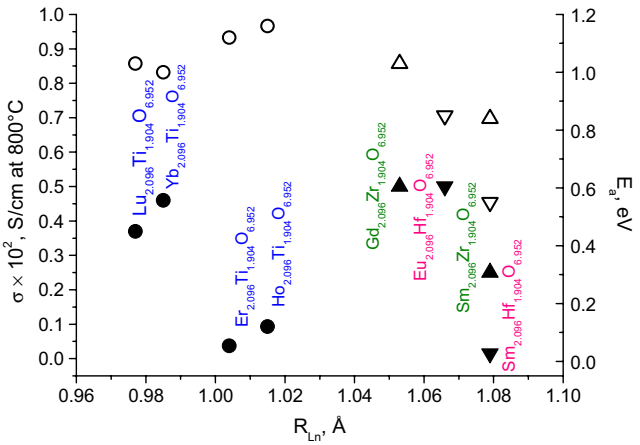

Fig. 7 Ionic conductivity (*filled data points*) and activation energy (*open data points*) as functions of the radius of the lanthanide for $Ln_{2.096}Hf_{1.904}O_{6.952}$ (Ln = Sm–Lu; M = Ti, Zr, Hf)

phases $Ln_{2+x}M_{2-x}O_{7-\delta}$ (M = Zr, Hf), as well as that of heavily doped fluorite-like phases at the phase boundary of $Ln_{2+x}M_{2-x}O_{7-\delta}$ (M = Zr, Hf), is always lower than the conductivity of the disordered pyrochlores.

Some factors, which may effect on the oxide ion conductivity of pyrochlore-like $Ln_{2+x}M_{2-x}O_{7-\delta}$ (Ln = Sm–Lu; M = Ti, Zr, Hf; M = 0–0.81) are discussed.

Acknowledgements This work was supported by the Presidium of the Russian Academy of Sciences (program "Synthesis of Inorganic Substances with Controlled Properties and Fabrication of Related Functional Materials," grant no. 18P/2009), the Russian Foundation for Basic Research (grant no. 07-03-00716), the Department of Materials Sciences of the Russian Academy of Sciences (program of the Basic Investigations of New Metal, Ceramic, Glass- and Composite-Materials and the Deutsche Forschungsgemeinschaft (grant no. CZ 436RUS17/96/06).

References

1. M.P. van Dijk, K.J. de Vries, A.J. Burggraaf, Solid State Ion **9/10**, 913 (1983). doi:10.1016/0167-2738(83)90110-8
2. T. van Dijk, K.J. de Vries, A.J. Burggraaf, Phys. Status Solidi (a) **58**, 115 (1980). doi:10.1002/pssa.2210580114
3. T. Takahashi, H. Iwahara, Y. Nagai. J. Appl. Electrochem. **2**, 97 (1972). doi:10.1007/BF00609125
4. V.V. Kharton, A.A. Yaremchenko, E.N. Naumovich, F.M.B. Marques, J. Solid State Electrochem. **4**, 243 (2000). doi:10.1007/s100080050202
5. G.V.M. Kiruthika, K.V. Govindan Kutty, U.V. Varadarju, Solid State Ion. **110**, 335 (1998). doi:10.1016/S0167-2738(98)00140-4
6. B.J. Wuensch, K.W. Eberman, C. Heremans, E.M. Ku, P. Onnerud, E.M.E. Yeo, S.M. Hail, J.K. Stalick, J.D. Jorgensen, Solid State Ion. **129**, 111 (2000). doi:10.1016/S0167-2738(99)00320-3
7. K.J. Moreno, A.F. Fuentes, J. Garcia-Barriocanal, C. Leon, J. Santamaria. J. Solid State Chem. **179**, 323 (2006). doi:10.1016/j.jssc.2005.09.036
8. K.J. Moreno, M.A. Guevara-Liceaga, A.F. Fuentes, J. Garcia-Barriocanal, C. Leon, J. Santamaria. J. Solid State Chem. **179**, 928 (2006). doi:10.1016/j.jssc.2005.12.015
9. A.V. Shlyakhtina, M.V.Boguslavskii Knotko, S.Y. Stefanovich, I. V. Kolbanev, L.L. Larina, L.G. Shcherbakova, Solid State Ion. **178**, 59 (2007). doi:10.1016/j.ssi.2006.11.001
10. P.Y. Butyagin, I.K. Pavlichev, React. Solids **1**, 361 (1986). doi:10.1016/0168-7336(86)80027-4
11. D. Michel, M. Perez, Y. Jorba, R. Collongues, Mater. Res. Bull. **9**, 1457 (1974). doi:10.1016/0025-5408(74)90092-0
12. M.P. van Dijk, F.C. Mijlhoff, A.J. Burggraaf, J. Solid State Chem. **62**, 377 (1986). doi:10.1016/0022-4596(86)90253-7
13. T. Uehara, K. Koto, F. Kanamaru. Solid State Ion. **23**, 137 (1987). doi:10.1016/0167-2738(87)90093-2
14. A.V. Shlyakhtina, D.A. Belov, O.K. Karyagina, L.G. Shcherbakova. J. of Alloys and Compounds, published on line 25.12.2008
15. H. Takamura, H.L. Tuller, Solid State Ion. **134**, 67 (2000). doi:10.1016/S0167-2738(00)00715-3
16. K.W. Eberman, B.J. Wuensch, J.D. Jorgensen, Solid State Ion. **148**, 521 (2002). doi:10.1016/S0167-2738(02)00099-1
17. A.V. Shlyakhtina, A.V. Knotko, M.V. Boguslavskii, S.Y. Stefanovich, D.V. Peryshkov, I.V. Kolbanev, L.G. Shcherbakova, Solid State Ion. **176**, 2297 (2005). doi:10.1016/j.ssi.2005.06.005
18. A.F. Fuentes, K. Boulahya, M. Maszka, U. Amador. Solid State Sci. **7**, 343 (2005). doi:10.1016/j.solidstatesciences.2005.01.002
19. M. Pruneda, E. Artacho. Phys. Rev. B **72**, 08510 (2005). doi:10.1103/PhysRevB.72.085107